JOURNAL OF MATERIALS SCIENCE 32 (1997) 235–243

# Toughening of calcium hydroxyapatite with silver particles

X. ZHANG, G. H. M. GUBBELS, R. A. TERPSTRA, R. METSELAAR
*Centre for Technical Ceramics, P.O. Box 513, 5600 MB Eindhoven, The Netherlands*

Calcium hydroxyapatite bioceramic was toughened by preparing composites with silver particles as reinforcements. The composites were fabricated from hydroxyapatite and silver oxide raw powders. The sintering behaviour was investigated using dilatometry. An optimized sintering programme was designed to promote densification and to suppress the decomposition of the hydroxyapatite matrix and the evaporation of silver. High density was achieved on both small cylinder samples and large block samples by pressureless sintering. The density of the composites is over 92.4% theoretical with silver inclusions up to 30 vol %. The strength of the composites is greater than 80 MPa as tested by four-point bending. Silver inclusions improve the toughness consistently, from 0.70 MPa $m^{1/2}$ for the monolithic hydroxyapatite to 2.45 MPa $m^{1/2}$ at 30 vol % silver. Studies on the toughening mechanism indicate that crack bridging and subsequent plastic work of silver are mostly responsible for the toughening, whereas crack deflection also makes some contribution.

## 1. Introduction

Studies on the mechanical properties of calcium hydroxyapatite ($Ca_{10}(PO_4)_6(OH)_2$; HAp) ceramics have progressed with the aim of overcoming the inherent brittleness and realizing the practical use of HAp as bioactive load-bearing implant materials [1, 9]. By preparing composite materials, some improvement has been demonstrated in the fracture toughness of the HAp ceramics. Various reinforcements have been tried, e.g. FeCr alloy fibres [2], carbon fibres [3], $Si_3N_4$ whiskers [5], $Al_2O_3$ whiskers [5] or platelets [6], SiC platelets [5] and $ZrO_2$ particles [3, 5, 7]. In many cases the composites cannot be successfully prepared and their mechanical properties cannot be characterized.

The general problems associated with the fabrication of the HAp-based composites are: (1) the low density and the presence of defects (cracks); (2) the degradation of the reinforcements due to severe reactions with the HAp matrix; and (3) the dehydration and decomposition of the HAp caused by the sintering atmosphere and the presence of the reinforcements. As far as the HAp matrix is concerned, the following reactions can be written

$$Ca_{10}(PO_4)_6(OH)_2 \rightarrow Ca_{10}(PO_4)_6(OH)_{2-2x}O_x\square_x + xH_2O(g) \quad (1)$$

$$Ca_{10}(PO_4)_6(OH)_{2-2x}O_x\square_x \rightarrow 2Ca_3(PO_4)_2 + Ca_4P_2O_9 + (1-x)\,H_2O(g) \quad (2)$$

where $\square$ denotes the vacancies at OH lattice sites. In dehydration, HAp loses OH radicals and forms oxyhydroxyapatite (OHA). During decomposition, OHA further transforms to tricalcium phosphate ($Ca_3(PO_4)_2$, TCP) and tetracalcium phosphate ($Ca_4P_2O_9$). To suppress the reactions and to help the densification, some complicated techniques, e.g. hot (isostatic) pressing, have been employed.

Recently, we have used silver particles to reinforce HAp [10, 11]. The idea is to take advantage of the ductility of silver according to the crack-bridging mechanism [12, 13]. Some toughening effect has been achieved in our previous studies. The selection of silver as the reinforcement is also based on the consideration that silver is inert and has anti-bacterial properties [14, 15]. HAp with silver absorption (concentration up to 4 $\mu g\,mg^{-1}$) exhibits very similar behaviour to the control HAp, with remarkably good osteoconduction and incorporation in bone *in vivo* implantation. Further, silver has a higher thermal expansion coefficient than HAp ($15 \times 10^{-6}\,K^{-1}$). This is preferred because compressive stress will be introduced into the HAp matrix when cooling down from the sintering temperature. In addition, no chemical reaction between HAp and silver is expected in oxygen-containing atmospheres at normal pressure. The composites can be sintered in (moist) air and consequently the dehydration or decomposition of the HAp matrix can be suppressed. The use of silver as a reinforcement in HAp was also reported in a recent paper [16]. The hardness and the strength of the composites were given (with highest strength as 75 MPa at 10 vol % Ag), but the elastic modulus and the fracture toughness, which are very important parameters for the application of HAp, were not mentioned. The present paper reports a systematic investigation on the sintering behaviour and the mechanical properties of the HAp matrix composites.

0022–2461  

## 2. Experimental procedure

### 2.1. Raw materials and powder processing

HAp powder (Ca/P = 1.62, Merck A.G., Darmstadt, Germany) was used in the present study. The powder has a specific surface area of $67 \pm 3\ m^2\ g^{-1}$ as measured with standard $N_2$-BET equipment. The powder has a very poor packing density. Preliminary study with this powder often showed problems such as an irregular shape and low density of green bodies after cold isostatic pressing, and cracks in sintered samples. To solve these problems, the as-received powder was heat treated (calcined) at 1000 °C in air. After this treatment, the powder has a median size of about 0.60 μm and a specific surface area of $11.0 \pm 0.6\ m^2\ g^{-1}$. The calcined powder exhibits a good flowability, suitable for further processing.

Silver oxide powder ($Ag_2O$, > 99 %, Sigma-Aldrich, Belgium) was chosen as the starting raw material to produce silver. This is advantageous because $Ag_2O$ powder is easy to modify by conventional milling techniques. The silver particle size can be controlled and a homogeneous dispersion of silver particles in the HAp matrix can be achieved.

Powder blends, which have final compositions of 0, 5, 10, 20 and 30 vol % silver, were prepared by ball milling appropriate amounts of the calcined HAp powder together with the $Ag_2O$ powder for 48 h in a polyethylene bottle with $Si_3N_4$ balls (hot-pressed, ~11 mm diameter × 11 mm cylinders) and distilled water. After milling, the slurry was dried and sieved through a 250 μm sieve, resulting in good flowability. Powder compacts were fabricated by cold isostatic pressing at 250 MPa in the shape of cylinders (10 mm diameter × 10 mm) for dilatometer investigation and blocks (14 mm × 22 mm × 56 mm) for mechanical testing.

### 2.2. Sintering

Sintering was carried out at 1250 °C for 1 h in air. The choice of this temperature is based on early work done in this laboratory [17] and on data from the literature [1]. To study the sintering process of both monolithic HAp and composites with various silver contents, dilatometer experiments were performed. A simple sintering programme was adopted with a heating and cooling rate of $10\ °C\ min^{-1}$, a peak temperature of 1250 °C, and a soaking time of 1 h. Based on the results of the dilatometer investigation, the large block samples were sintered following an optimized firing programme (Section 3.2).

### 2.3. Characterization

The density of sintered samples was measured using the Archimedes method. To study the evaporation of silver and dehydration of the HAp matrix, the weight loss of the samples after sintering was monitored. The phases present in the composites were analysed on cut and ground surfaces using X-ray diffraction (XRD). To evaluate the extent of the decomposition of the HAp, the intensity ratio of the strongest peaks of β-TCP (0 2 10) and HAp (2 1 1) was compared. The microstructure was observed on polished and etched surfaces using scanning electron microscopy (SEM). Etching was done by immersing the specimens into a 1 wt % citric acid solution for 1–2 min. The average matrix grain size and silver particle size were measured according to the linear intercept method counting more than 200 grains and 100 particles.

The Vickers' hardness was tested on polished surfaces under a load of 19.6 N. The elastic modulus of the materials was measured using the resonance method (Grindosonic) and from the force-displacement relation obtained from a four-point bending test. The displacement was measured differentially using three pins touching the bar symmetrically at the bottom [18]. Test bars with dimensions of 3 mm × 4 mm × 45 mm were machined from the sintered block-shaped samples. Four-point bending tests were performed to determine the fracture strength and toughness. For the strength measurement, the inner and outer span were 20 and 40 mm respectively, and the loading rate was $0.5\ mm\ min^{-1}$. For the toughness measurement, a Chevron notch was introduced into each bar. The loading was on a span of 5/20 mm at a rate of $1\ \mu m\ s^{-1}$. Six measurements were performed for each material in order to obtain an average value of strength or toughness. The fracture surfaces of the samples were examined by SEM. To understand the toughening mechanism, Vickers' indentations were made on the polished surfaces and the crack propagation path was studied.

## 3. Results and discussion

### 3.1 Dilatometer investigation

The sintering in a dilatometer was carried out in air for technical convenience. The relative shrinkage, $\Delta L/L$, and the shrinkage rate, $dL/Ldt$, as a function of time (temperature) are illustrated in Fig. 1. In both monolithic HAp and Ag/HAp composite samples, the sintering starts at about 800 °C. Large shrinkage occurs in the temperature range from 1000–1200 °C, corresponding to a high sintering rate. The densification proceeds with very low sintering rate during the soaking period at 1250 °C. Comparing the monolithic HAp with the composites, the HAp sample shows a first shrinkage rate peak at about 1020 °C. This peak is probably related to dehydration which starts at about 800 °C, as revealed by our thermogravimetric (TG) and differential thermal analyses (DTA) [19]. The OHA formed by dehydration accelerates the densification [9]. The composite samples show a lower sintering rate at about 960 °C. This is caused by the expansion of silver which melts at this temperature. The first shrinkage peak caused by the dehydration becomes less clear because of the expansion of molten silver. It should be pointed out that, although silver is in the liquid form, the sintering is not liquid-phase sintering in the usual sense, because the mechanism of solution and precipitation does not occur in the sintering process of the composites.

After sintering in the dilatometer, a reasonably high density was realized for all the samples, as illustrated in Fig. 2. The decomposition of the HAp matrix was

evaluated. Fig. 3 shows the XRD diffraction patterns of the composites. The relative composition of HAp and β-TCP in these samples is reflected in Fig. 4. Compared to the calcined HAp starting powder, the content of β-TCP increases in all the samples. However, up to 20 vol % Ag, the degree of decomposition is similar. Only at a higher silver content does the decomposition become significant.

Analysis of the microstructure of the composites showed a homogeneous dispersion of silver particles in the HAp matrix and a regular HAp grain distribution, as illustrated in Fig. 5. No abnormal grain growth of HAp was found, different from a literature observation [16]. The silver particles accumulate at the matrix grain boundaries (junctions). No reaction can be seen between silver and HAp. Up to 30 vol % Ag inclusions the silver phase remains discrete. This has been confirmed by electrical conductivity

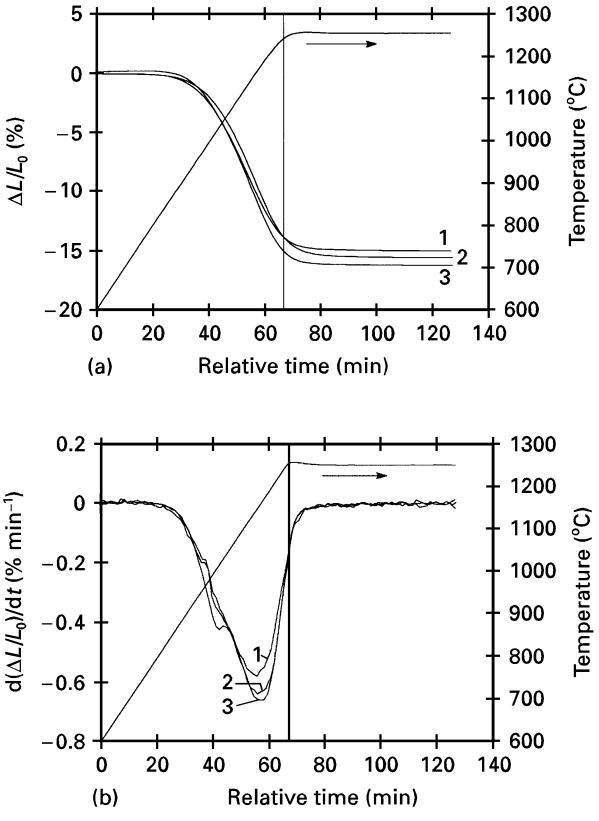


*Figure 1* (a) Relative shrinkage of the samples during sintering. (b) Shrinkage rate at various sintering times (temperatures). 1, 20 vol % Ag; 2, 10 vol % Ag; 3, HAp.

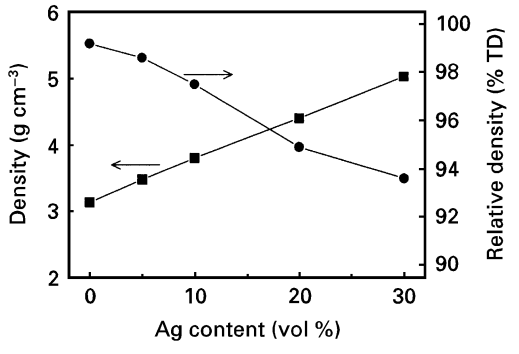


*Figure 2* Density of the samples after dilatometer experiments.

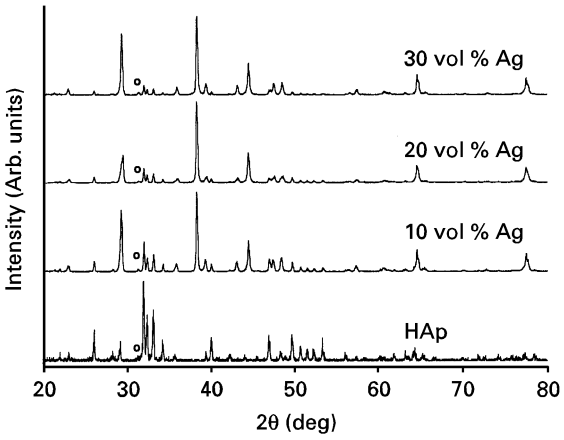


*Figure 3* Cu$K_\alpha$–XRD patterns of the monolithic HAp and the Ag/HAp composites. (○) The position of the strongest peak of β-TCP.

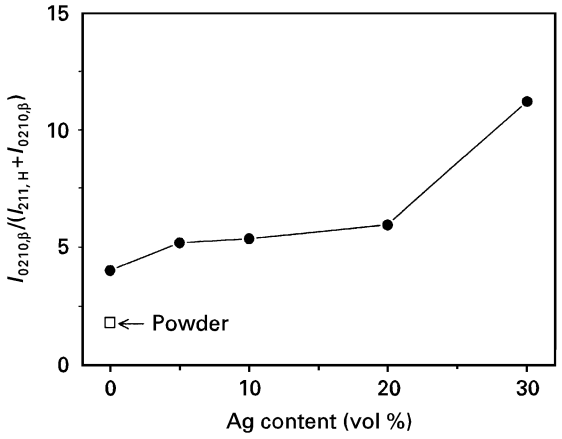


*Figure 4* Intensity ratio of XRD peaks of β-TCP (0 2 10) and HAp (2 1 1) in the samples.

measurements on thin disc samples (8 mm diameter × 0.8 mm) with silver electrodes. The discontinuity of the silver phase at such a high concentration is closely related to the non-wetting character of molten silver on HAp. The wetting angle was measured to be about 130°, as shown in Fig. 6, in which silver drops formed on a surface after sweating-out from the interior. Sweating was only observed in the 30 vol % Ag samples. However, in all other composite samples, a 10–20 μm wide silver depleted zone at the edges was always observed. This was caused by the silver evaporation during sintering. The molten silver has a high vapour pressure at the sintering temperature.

The average HAp grain size and the silver particle size have been measured. Fig. 7 shows that the grain growth of the HAp is not strongly inhibited. One reason is that the molten silver can exert only very limited stress on the matrix. The mechanism hindering the grain growth is probably that silver particles (melts) act as barriers for the diffusion of HAp atoms. As expected, the silver particle size increases with increasing contents. Most of the particles have a size of a few micrometres, but occasionally very large silver particles (as large as 100 μm) can be observed. It is not

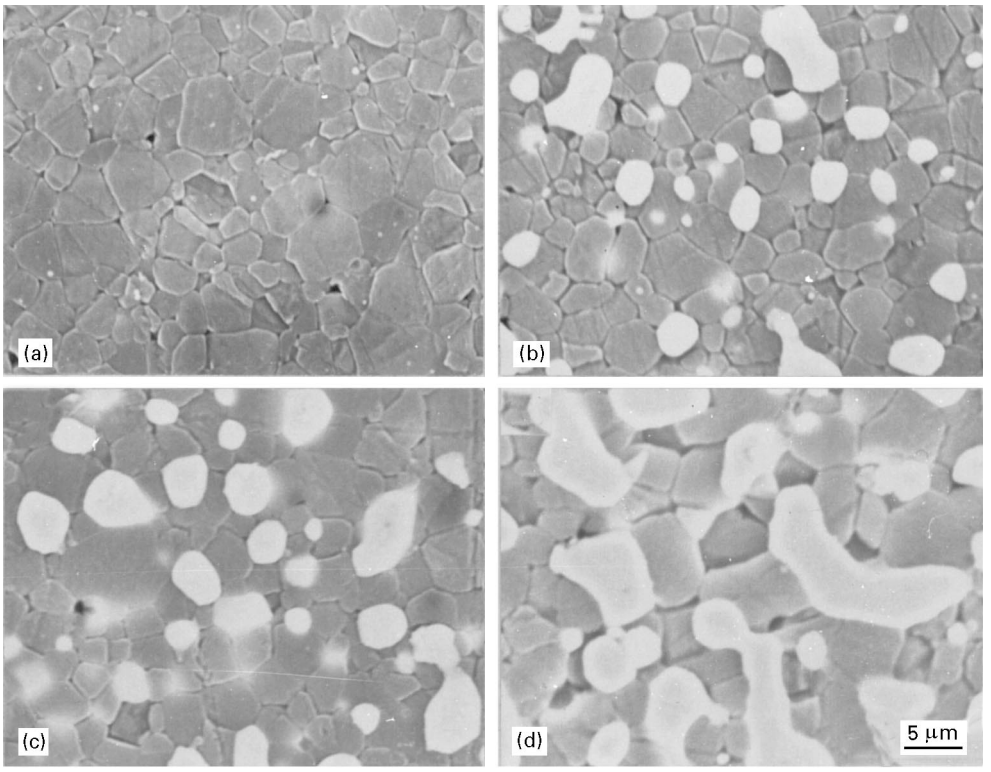


*Figure 5* Microstructure of the HAp and the Ag/HAp composites after etching: (a) monolithic HAp, (b) 10 vol % Ag, (c) 20 vol % Ag, and (d) 30 vol % Ag.

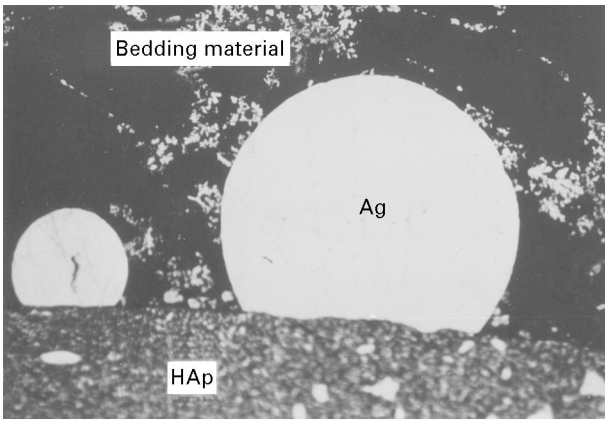


*Figure 6* Silver drops formed on the 30 vol % Ag sample surface showing the poor wettability of molten silver on HAp.

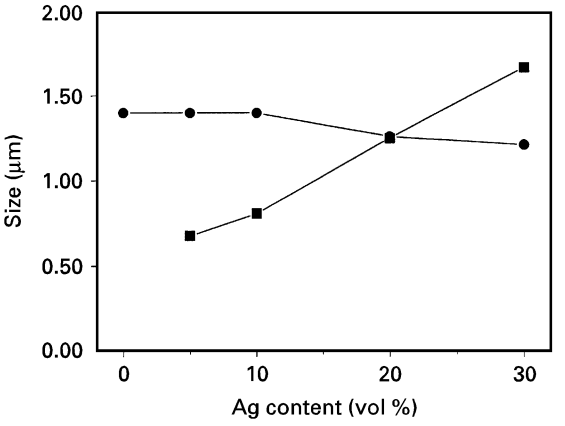


*Figure 7* (■) Average silver particle size and (●) HAp grain size in the materials at various compositions.

clear whether they were introduced by agglomeration during powder processing or by coalescence of the molten silver at the low-density stage during sintering.

## 3.2. Sintering of large block samples

In the sintering of the large block-shaped samples, several factors should be considered. Firstly, compared to small cylinder samples, a longer densification time is required. Secondly, to diminish the evaporation of silver, a low sintering temperature and a short holding time are preferred. Thirdly, as the $Ag_2O$ in the powder compacts decomposes and releases oxygen at about 180 °C (detected by TG/DTA analyses), the heating rate around this temperature should be low. Fourthly, the thermoshock resistance of the monolithic HAp is very poor (due to its high thermal expansion coefficient, low strength and low toughness [19]), so the samples after sintering have to be cooled down very slowly. The critical cooling rate, $dT/dt$, can be estimated from the third thermoshock factor ($R_s''$) [20]

$$\left(\frac{dT}{dt}\right)_{max} = R_s''\left(\frac{3}{r_m^2}\right) = \left(\frac{\lambda}{\rho C_p}\right)\left[\frac{\sigma(1-\nu)}{\alpha E}\right]\left(\frac{3}{r_m^2}\right) \quad (3)$$

where $\lambda$ is the thermal conductance, $\rho$ the density, $C_p$ the heat capacity, $\nu$ Poisson's ratio, $E$ the elastic modulus, $\alpha$ the thermal expansion coefficient, $\sigma$ the fracture strength, and $r_m$ the sample diameter. For HAp, using $\sigma = 100$ MPa, $E = 117$ GPa, $\nu = 0.28$, $\alpha = 15 \times 10^{-6}\ K^{-1}$, $\lambda = 1.3\ J\,s^{-1}\,m^{-1}\,K^{-1}$, $\rho = 3.16$

$g\,cm^{-3}$, $C_p = 0.765\,J\,K^{-1}\,g^{-1}$, and $r_m = 5$ cm, a critical cooling rate of about $1.5\,^{\circ}C\,min^{-1}$ is obtained.

Taking these factors into account, an optimized sintering programme was designed based on the dilatometer experiments, as illustrated in Fig. 8. The heating is kept slow in the temperature range in which a high sintering rate occurs, so the sintering can take the advantage of a high rate at a relatively low temperature. It is expected that continuous porosity will be eliminated at this stage so that the evaporation of silver can be confined only to the sample surfaces upon further firing. The temperature is increased to a maximum of 1250 °C to shrink closed pores, so achieving high density. A slow cooling is very critical for HAp. This is evinced by an exploratory experiment with a cooling rate of $5\,^{\circ}C\,min^{-1}$. Thermal stress-induced cracks are shown on surfaces of pure HAp. For the Ag/HAp composites, a higher cooling rate is allowed because of the improved thermal shock resistance due to the high thermal conductance of silver ($419\,J\,s^{-1}\,m^{-1}\,K^{-1}$). During sintering, moist air is used to suppress the dehydration of HAp.

Following this programme, the large blocks were densified to almost the same level as the small cylinders in the dilatometer experiments (Fig. 9). These results are quite promising because they are obtained by pressureless sintering. The sintering may be improved further, e.g. using the concept of rate-controlled sintering [21].

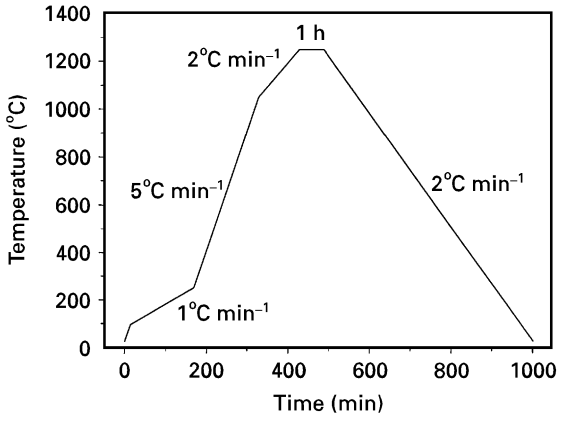


*Figure 8* The optimized sintering programme for the block samples.

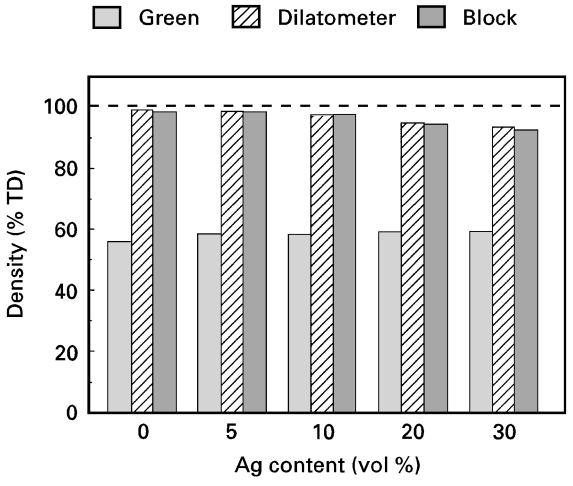


*Figure 9* Density of the block samples compared with that of dilatometer samples.

Fig. 10 compares the sintering weight loss of the dilatometer cylinders and the block samples. The blocks loose less weight than the cylinders, although the former are sintered for a longer time. Looking into the process, the weight loss is due to (1) the evaporation of the adsorbed water, (2) the dehydration of the HAp matrix, (3) the release of oxygen from $Ag_2O$, and (4) the evaporation of molten silver. The weight loss, $W_1$ due to the decomposition of $Ag_2O$ can be described as

$$W_1 = \frac{f\rho_{Ag}\dfrac{M_O}{2M_{Ag}}}{\left[f\rho_{Ag}\dfrac{M_{Ag_2O}}{2M_{Ag}} + (100 - f)\,\rho_{HAp}\right]} \quad (4)$$

where $f$ is the volume content of silver in the composites. The densities are $\rho_{Ag} = 10.5\,g\,cm^{-3}$, $\rho_{HAp} = 3.16\,g\,cm^{-3}$, while the molecular masses are $M_{Ag} = 107.9$, $M_O = 16.0$ and $M_{Ag_2O} = 231.8$. The results are shown as curve 1 in Fig. 10. Considering the weight loss of the monolithic HAp (on average about 1.6 %) and assuming that the matrix HAp in the composites has a similar behaviour, the total weight loss will be

$$W_1 = \frac{\left[f\rho_{Ag}\dfrac{M_O}{2M_{Ag}} + 1.60\,\%(100 - f)\rho_{HAp}\right]}{\left[f\rho_{Ag}\dfrac{M_{Ag_2O}}{2M_{Ag}} + (100 - f)\rho_{HAp}\right]} \quad (5)$$

The estimated values are indicated by curve 2 in Fig. 10. The extra weight loss over curve 2 should be attributed to the loss of silver, mostly by sweating at 30 vol % Ag. The increased dehydration at high silver contents (compared to pure HAp, see Fig. 4) makes only a minor contribution, because a complete dehydration of the matrix only results in maximally 1.8 wt % weight loss (the $H_2O$ content in HAp). It is noticed that the theoretical density is estimated from the nominal silver concentration. This estimated value is higher than the real one considering the loss of silver. Therefore, the relative density of the composites is larger than the values shown in Fig. 9.

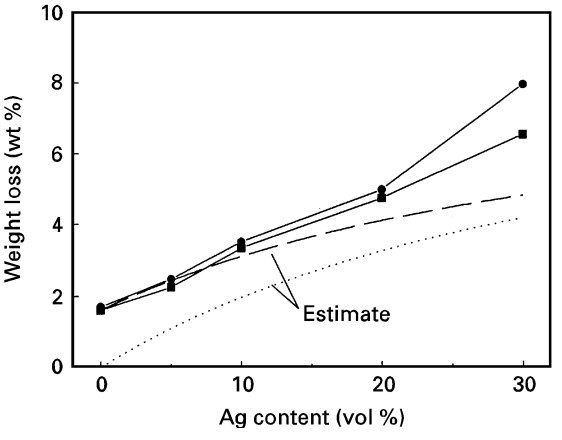


*Figure 10* Weight loss of the samples during sintering. Estimate 1 is based on the weight loss due to $Ag_2O$ decomposition, and estimate 2 due to both $Ag_2O$ decomposition and matrix weight loss. (●) Dilatometer, (■) Sintering. (····) Equation 4, (———) Equation 5.

TABLE I Mechanical properties of the HAp and Ag/HAp composites

| Sample | Hardness (GPa) | $E$ modulus (GPa) | | Strength, $\sigma_{4B}$ (MPa) | Toughness, $K_{Ic}$ (MPa m$^{1/2}$) |
|---|---|---|---|---|---|
| | | Resonance | Bending | | |
| HAp | 5.17 ± 0.18 | 112.0 | 101.1 | 38.8 ± 11.7 | 0.70 ± 0.09 |
| 5 vol % Ag | 4.51 ± 0.30 | 116.8 | 105.4 | 64.8 ± 16.4 | 0.95 ± 0.04 |
| 10 vol % Ag | 4.06 ± 0.11 | 112.1 | 100.4 | 100.7 ± 16.7 | 1.06 ± 0.06 |
| 20 vol % Ag | 2.89 ± 0.19 | 103.1 | 91.2 | 82.1 ± 9.4 | 1.49 ± 0.14 |
| 30 vol % Ag | 2.37 ± 0.09 | 88.4 | 80.9 | 80.0 ± 2.9 | 2.45 ± 0.21 |

## 3.3. Mechanical properties

The mechanical properties of the Ag/HAp composites are summarized in Table I.

### 3.3.1. Hardness and elastic modulus

In hardness measurements, the indentation diagonal size is around 100 μm, much larger than the silver inclusion size. Therefore, the hardness values are quite representative of the material property. Fig. 11 shows the hardness as a function of the silver content. The hardness decreases almost linearly with the increasing silver fraction, owing to the softness of silver and the increasing porosity.

Fig. 12 shows the elastic modulii of the materials measured by the ultrasonic pulse method and by the bending method. Data from the bend test are about 10% lower than the ultrasonic data; however, this seems to be inherent to the testing method [18]. For the monolithic HAp, the value of 112 GPa agrees well with the results obtained by De With *et al.* [1]. It should be mentioned, however, that a wide spread in the data is reported in the literature, ranging from 41–121 GPa [22]. The estimates are from the law of mixtures (namely, the upper limit of elastic modulus), assuming silver and HAp as laminates oriented parallel to an applied uniaxial stress and undergoing the same strain. Estimate 1 is obtained from

$$E = (1 - f)\, E_{\mathrm{HAp}} + f E_{\mathrm{Ag}} \tag{6}$$

using $E_{\mathrm{HAp}} = 117$ GPa and $E_{\mathrm{Ag}} = 76$ GPa at silver volume fraction, $f$, from 0%–30%. Estimate 2 further includes the influence of porosity. It is known that in the particular case of sintered HAp, the modulus is empirically related to the porosity, $p$, by [1]

$$E_{\mathrm{HAp}} = 117(1 - 2.01p) \tag{7}$$

Thus, for the composites

$$E_{\mathrm{HAp}} = 117(1 - 2.01p)\,(1 - f) + 76f \tag{8}$$

In general, silver inclusions lower the modulus of the materials, but at 5 vol % Ag an increase is observed and the reason is not clear. The decrease in the elastic modulus of Ag/HAp composites is desirable from the viewpoint of bio-applications [23]. Because the modulus of natural bones is low (7–25 GPa) [24], an implantation with high modulus can cause severe stress concentrations, i.e. load shielding from a natural bone, which may weaken the bone and deteriorate the implant/bone interface [25]. In fact, the high modulus is one of the drawbacks for alumina ($E_{Al_2O_3} = 380$ GPa) and zirconia ($E_{ZrO_2} = 210$ GPa) in orthopaedic applications.

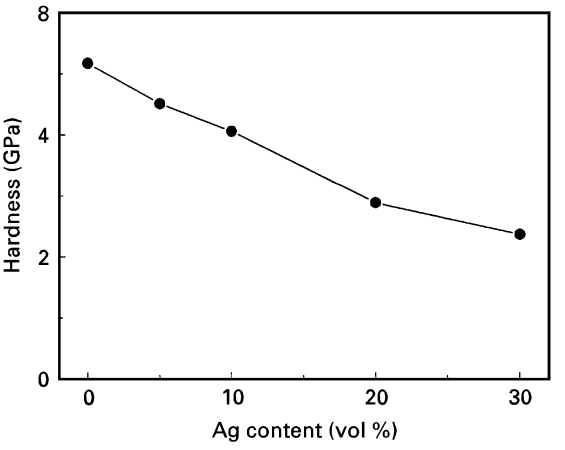


*Figure 11* Vickers' hardness of the HAp and the Ag/HAp composites. $H_V$ at load of 19.6 N.

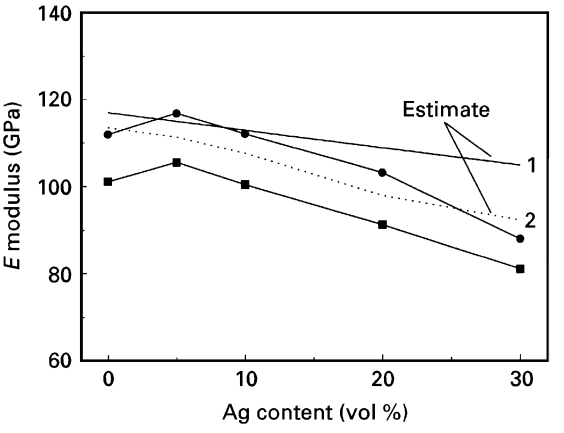


*Figure 12* Elastic modulus of the HAp and the Ag/HAp composites. Estimate 1 is based on the law of mixtures and estimate 2 further considers the effect of porosity. (●) Grindosonic, (■) bending. (——) Equation 6, (····) Equation 8.

### 3.3.2. Strength

The strength of the materials is shown in Fig. 13. The strength data for monolithic HAp and for 5 vol % Ag/HAp composite are not very reliable, because large machining defects were found on the surfaces of the bending bars. These defects are chips broken away from bar samples during machining and cracks caused by heating and cooling during fixing samples with

binder. Machining defects are also found on the 10 vol % Ag/HAp samples but are much less severe. As can be noticed from the error bars, the standard deviations of the measurements are large for the 0, 5 and 10 vol % Ag samples, but become small for the 20 and 30 vol % Ag samples. Therefore, the inclusion of silver has improved the machinability of the HAp.

Literature data show that the strength of sintered HAp varies from about 30–177 MPa, depending on both material processing and testing methods [8, 17]. With the same powder as used in the present study, strengths as high as 115 MPa were achieved on pressurelessly sintered HAp [1]. Adopting this value as the strength of the present monolithic HAp, the strength of the composites seems to decrease with the increasing silver contents. At 30 vol % Ag the composite has a strength of 80 MPa. Compared to the literature [16], the present results are quite promising.

Fractography shows that fracture origins are difficult to identify except for the HAp and 5 vol % Ag/HAp samples, in which the machining defects are the critical flaws. In the 10, 20 and 30 vol % Ag samples, some large intrinsic defects are observed, such as silver or matrix agglomerates about 100 μm in size, which may be responsible for the fracture. The critical defect size, $a_c$, in the samples can be estimated by applying the fracture mechanics formula (Griffith relation)

$$a_c = \left(\frac{K_{Ic}}{Y\sigma}\right)^2 \tag{9}$$

where $Y = 1.26$, the appropriate value for semicircular surface defects [26]. Using the experimental toughness, $K_{Ic}$, and strength, σ, data, the calculated defect size is extremely large, 207 and 591 μm for the 20 and 30 vol % Ag samples, respectively. This is related to the increased possibilities of large silver agglomerates and coalescences because of the decreased mean free path between particles at such high silver concentrations. With improved processing, the defect size can be diminished to some extent. By slip casting, very high strength has already been obtained on monolithic HAp samples [17]. This is also predicted for Ag/HAp composites at low silver concentrations because the distribution of silver (in fact $Ag_2O$) can be further homogenized and agglomeration can be avoided. At high silver concentrations, in addition to improving the distribution in the green state, the possible coalescence at sintering should also be prevented. Therefore, the sintering should be conducted at temperatures lower than the melting point of silver. However, this requires very active HAp powders combined with hot (isostatic) pressing. The present HAp powder can be densified at 1000–1050 °C by hot-pressing [2], still higher than the melting point of silver.

### 3.3.3. Fracture toughness

The fracture toughness and the work of fracture are shown in Fig. 14. The work of fracture (or strain energy release rate) $G_{Ic}$ is calculated from the toughness and elastic modulus according to the formula

$$G_{Ic} = \frac{K_{Ic}^2}{E} \tag{10}$$

Monolithic HAp has a very low toughness, 0.70 MPa $m^{1/2}$, showing that the material is very brittle. The inclusion of silver particles has consistently improved the toughness of HAp. At 30 vol % Ag, the toughness is 2.45 MPa $m^{1/2}$, namely 3.5 times that of the monolithic HAp. Owing to the increase in toughness but decrease in elastic modulus, a higher magnitude of the work of fracture is achieved, five times at 20 vol % Ag and 15 times at 30 vol % Ag, compared to that of the monolithic HAp. From the energy point of view, the 30 vol % Ag composites are twice as fracture resistant as a normal alumina ($E = 380$ GPa and $K_{Ic} = 3.8$ MPa $m^{1/2}$).

The toughening mechanism was investigated by examining the indentation crack path as shown in Fig. 15. The HAp shows a transgranular fracture behaviour, indicating that the toughness of HAp is independent of its grain size. Because of this transgranular fracture character, very straight cracks are often observed radiating from indentation corners, as shown in Fig. 15b for the sample with 30 vol % Ag. The crack is deflected when it encounters silver particles. Sometimes crack bridging occurs and bridging silver particles stretch plastically. Therefore, the toughening is attributed to both crack deflection and crack bridging at sites of silver particles. The contribution of crack

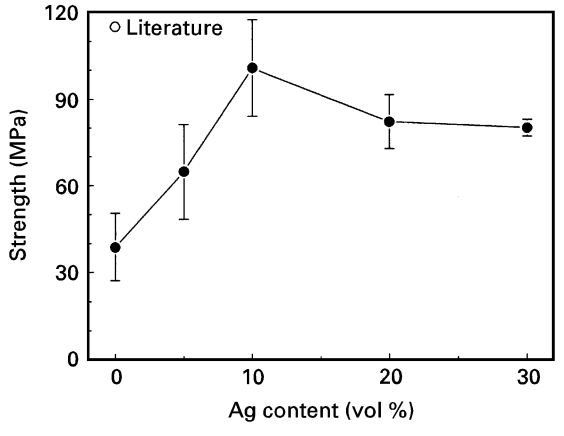


*Figure 13* Strength of the HAp and the Ag/HAp composites. The literature data are from de With *et al.* [1]

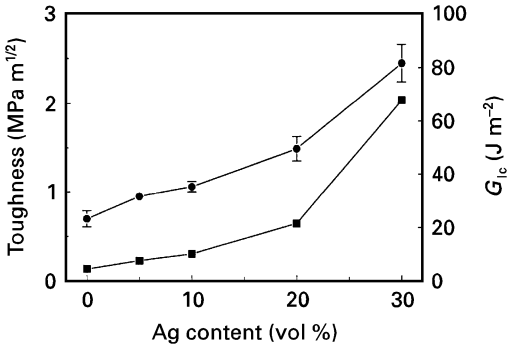


*Figure 14* (●) Toughness and (■) work of fracture of the HAp and the Ag/HAp composites.

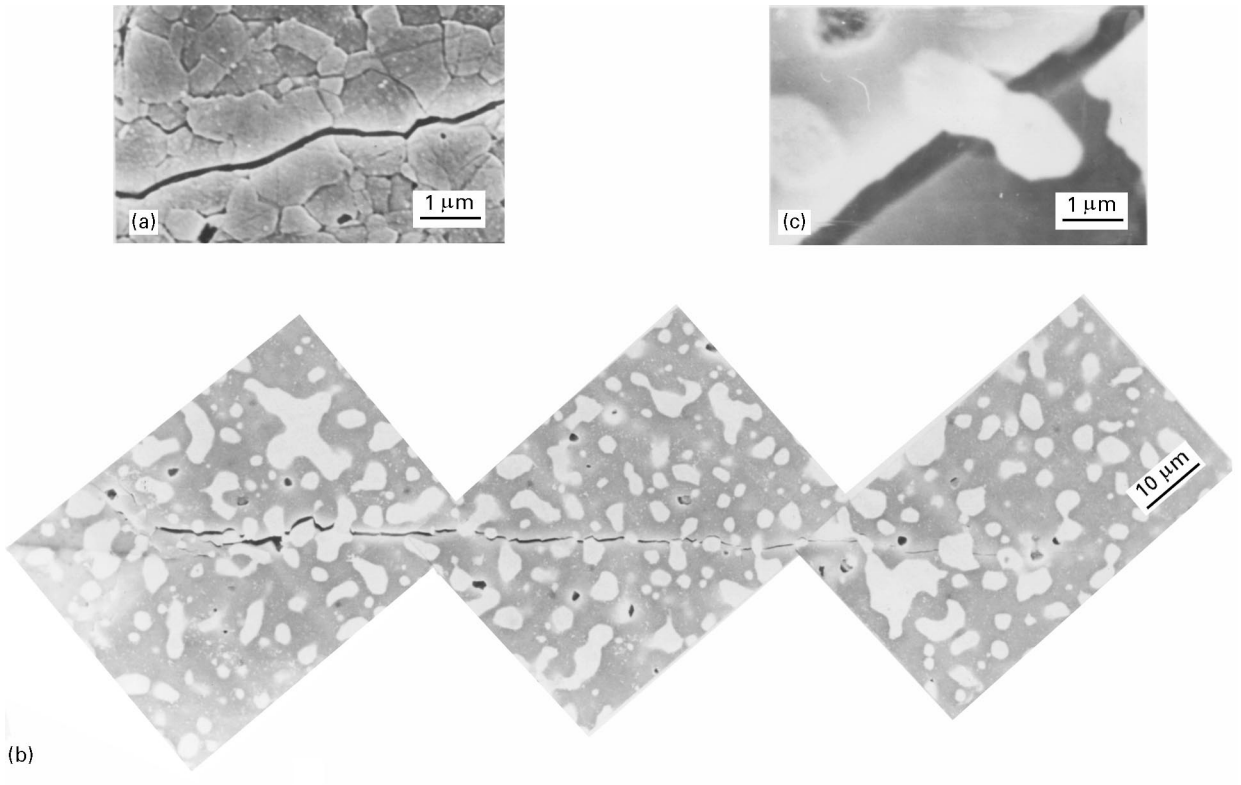


*Figure 15* (a) Transgranular fracture character of HAp, (b) indentation crack propagation pattern in the 30 vol % Ag/HAp composite, and (c) crack bridging and plastic stretching of a silver particle.

deflection can be predicted according to a model [27], to be only about 22 %–35 % of the *matrix* toughness, $G_m$, at 5–30 vol % particle inclusions. Thus, the crack bridging and the stretching of silver particles seem to be more important to toughening.

The toughening due to crack bridging can be obtained by subtracting the matrix toughness and the deflection contribution

$$\Delta G_c = G_c - G_m(1 - f) - \Delta G_{c,\,\text{deflection}} \qquad (11)$$

According to the crack-bridging model [12, 13], $\Delta G_c$ can also be expressed as

$$\Delta G_c = f\sigma_0 R\chi \qquad (12)$$

where $f$ is the area fraction of ductile reinforcement on the fracture surface, $\sigma_0$ is the uniaxial yield strength, $R$ is the cross-sectional radius of the reinforcement, and $\chi$ is a work of rupture parameter which represents the toughening capacity of the reinforcement. The value of $\chi$ is related to the details of the interface debonding and the plastic stretching of the ductile reinforcement during fracture [12, 13].

The increase in toughness, $\Delta G_c$, is plotted as a function of $fR$, as shown in Fig. 16. Between the compositions of 5, 10 and 20 vol % Ag, almost a straight line can be drawn as predicted from the crack-bridging model. The prominent toughening at 30 vol % Ag is related to the morphology of silver reinforcements. Detailed examination shows that a crack tends to stretch and eventually fracture an elongated particle when it approaches the particle in the cross-longitudinal direction (Fig. 15c). When approaching a round-shaped particle or an elongated particle in the longitudinal direction, a crack is likely to be deflected.

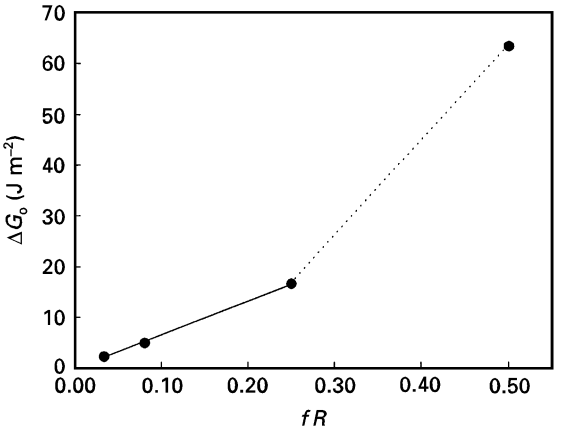


*Figure 16* Toughness increment as a function of volume fraction and particle size of silver reinforcements.

With the increasing silver content, more elongated silver particles are formed. This is especially obvious in the 30 vol % Ag composites.

### 3.3.4. Opportunities for further toughening

The Ag/HAp interface shows no reactions and the bonding appears to be weak as indicated by the crack propagation along the interface. If the interface bonding can be improved, the plastic deformation of silver may act more effectively as an energy-absorbing mechanism and toughen the material further. Adding titanium to silver may be a solution to improve interfacial strength, but sintering could be a problem because of the high oxygen affinity of titanium. Preliminary study showed very severe titanium oxidation

and the presence of cracks between titanium oxide and HAp in a HAp/Ag–4Ti/HAp diffusion couple experiment in vacuum. Vacuum and reducing atmospheres are not preferred, owing to the instability of HAp.

On the other hand, because the HAp matrix is also very weak, a crack may easily be deflected into the matrix when encountering a reinforcement. Therefore, improving the inclusion/matrix interface bonding may not increase the crack resistance very much provided the inclusions are round shaped. A better approach is probably to improve the silver distribution, e.g. in a continuous network as in the WC/Co system, or in a sufficiently complex shape, or in a fibrous form with a high aspect ratio. This is obviously difficult to realize for silver reinforcements unless the sintering temperature can be lowered to below the melting point of silver.

## 4. Conclusion

Ag/HAp composite materials were prepared using HAp and $Ag_2O$ raw powders. The sintering behaviour of the composites was investigated using dilatometry. Large-sized samples were sintered to high density by pressureless sintering at 1250 °C in air following an optimized heating programme. The composite materials have homogeneous microstructures with fine silver particles well dispersed in the HAp matrix. Up to 20 vol % Ag addition, the decomposition of HAp to TCP in the composites is limited. The incorporation of silver leads to a decrease in the elastic modulus of the materials, which is desirable considering the analogy of natural bones. The fracture strength of the composites is greater than 80 MPa and the strength can be improved by applying refined processing techniques. The fracture toughness is consistently improved with increasing silver inclusions. At 30 vol % Ag the composite has a toughness, $K_{Ic}$, 3.5 times that of the matrix, and a work of fracture twice that of alumina. The toughening is partly due to crack deflection and mostly due to crack bridging at silver particles. The bridging effect is especially prominent at high silver concentrations where elongated silver particles are formed.

## References


1. G. DE WITH, H. J. VAN DIJK, N. HATTU and K. PRIJS, *J. Mater. Sci.* **16** (1981) 1592.
2. G. DE WITH and A. J. CORBIJN, *ibid.* **24** (1989) 3411.
3. A. J. RUYS, K. A. ZEIGLER, B. K. MILTHORPE and C. C. SORRELL, in "Ceramics Adding the Value", "Proceedings of the International Ceramic Conference", Vol. 1, Australia, 1992, edited by M. J. Bannister (CSIRO Publication, Melbourne, 1992) p. 598.
4. T. NOMA, N. SHOJI, S. WADA and T. SUZUKI, *J. Ceram. Soc. Jpn.* **100** (1992) 1157.
5. M. YOSHIMURA, K. IOKU and S. SOMIYA, in "Euro-Ceramics", Vol. 3, "Engineering Ceramics", edited by G. de With, R. A. Terpstra and R. Metselaar (Elsevier Applied Science, London, 1989) p. 16.
6. HUAXIA JI and P. M. MARQUIS, *J. Mater. Sci.* **28** (1993) 1941.
7. M. TAKAGI, M. MOCHIDA, N. UCHIDA, K. SAITO and K. UEMATSU, *J. Mater. Sci., Mater. Med.* **3** (1992) 199.
8. A. ROYER, J. C. VIGUIE, M. HEUGHEBAERT and J. C. HEUGHEBAERT, *ibid.* **4** (1993) 76.
9. P. E. WANG and T. K. CHAKI, *ibid.* **4** (1993) 150.
10. X. ZHANG, G. H. M. GUBBELS, R. A. TERPSTRA and R. METSELAAR, in "Third Euro-Ceramics", Vol. 3, edited by P. Duran and J. F. Fernandez (Faenza, Editrice Iberica S.L., Castellon de la Plana, 1993) p. 31.
11. *Idem*, in "Proceedings of the 8th CIMTEC, Ceramics: Charting the Future, Advance in Science and Technology", edited by P. Vincenzini (Techna, Faenza, 1995) p. 2125.
12. L. S. SIGL, P. A. MATAGA, B. J. DALGLEISH and R. M. McMEEKING, *Acta Metall.* **36** (1988) 945.
13. M. F. ASHBY, F. J. BLUNT and M. BANNISTER, *ibid.* **37** (1989) 1847.
14. J. A. SPADARO, S. E. CHASE and D. A. WEBSTER, *J. Biomed. Mater. Res.* **20** (1986) 565.
15. J. A. SPADARO, R. J. DISTEFANNO and S. E. CHASE, in "The 17th Annual Meeting of the Society for Biomaterials", Scottsdale, Arizona, USA, 1–5 May 1991, edited by J. Russell Parsons (Society for Biomaterials, Newark, 1991) p. 52.
16. T. K. CHAKI and P. E. WANG, *J. Mater. Sci. Mater. Med.* **5** (1994) 533.
17. R. A. TERPSTRA, J. C. T. VAN DER HEIJDE, P. SWAANEN, X. ZHANG and G. GUBBELS, in "Third Euro-Ceramics", Vol. 3, edited by P. Duran and J. F. Fernandez (Faenza Editrice Iberica S.L., Castellon de la Plana, 1993) p. 61.
18. B. J. DE SMET, "Young's Modulus Measurements on an Alumina and a Borosilicate Bar Loaded in Three and Four Point Bending", Petten: Netherlands Energy Research Foundation ECN (ECN-I; 90041) (1990).
19. X. ZHANG, Thesis, Eindhoven University of Technology, The Netherlands (1994).
20. D. MUNZ and T. FETT, "Mechanische Verhalten keramischer Werkstoffe" (Springer Berlin, Germany, 1989).
21. H. PALMOUR III, M. L. HUCKABEE and T. M. HARE, in "Sintering – New Developments", edited by M. M. Ristic (Elsevier Science, Amsterdam, 1979) p. 46.
22. H. KAWAHARA, in "Ceramics in Surgery", edited by P. Vincenzini (Elsevier Science, Amsterdam, 1983) p. 49.
23. L. L. HENCH, *J. Am. Ceram. Soc.* **74** (1991) 1487.
24. T. KANAZAWA, "Inorganic Phosphate Materials" in "Materials Science Monographs" 52 Part (Elsevier, Amsterdam, 1989).
25. S. F. HULBERT, in "Proceedings of the 8th CIMTEC, Ceramics: Charting the Future, Advance in Science and Technology", edited by P. Vincenzini (Techna, Faenza, 1995).
26. G. K. BANSAL and W. H. DUCKWORTH, "Fracture Mechanics Applied to Brittle Materials", in ASTM STP 678, edited by S. W. Freiman (American Society for Testing and Materials, Philadelphia, PA, 1979) p. 38.
27. K. T. FABER and A. G. EVANS, *Acta Metall.* **31** (1983) 565.



*Received 15 February 1995*
*and accepted 2 July 1996*